CONFIDENTIAL

NASA TECHNICAL MEMORANDUM

UB
NASA TM X-1395

UB
NASA TM X-1395

CASE FILE
COPY

CONFIDENTIAL

LONGITUDINAL AERODYNAMIC CHARACTERISTICS OF THE APOLLO COMMAND MODULE AT A MACH NUMBER OF 20 AND DATA COMPARISONS OVER A WIDE MACH NUMBER-REYNOLDS NUMBER RANGE

by Julius E. Harris

Langley Research Center
Langley Station, Hampton, Va.

NATIONAL AERONAUTICS AND SPACE ADMINISTRATION • WASHINGTON, D. C. • JUNE 1967

CONFIDENTIAL

CONFIDENTIAL

NASA TM X-1395

NOFORN

LONGITUDINAL AERODYNAMIC CHARACTERISTICS OF THE APOLLO COMMAND MODULE AT A MACH NUMBER OF 20 AND DATA COMPARISONS OVER A WIDE MACH NUMBER-REYNOLDS NUMBER RANGE

By Julius E. Harris

Langley Research Center
Langley Station, Hampton, Va.

GROUP 4
Downgraded at 3 year intervals;
declassified after 12 years

CLASSIFIED DOCUMENT–TITLE UNCLASSIFIED
This material contains information affecting the national defense of the United States within the meaning of the espionage laws, Title 18, U.S.C., Secs. 793 and 794, the transmission or revelation of which in any manner to an unauthorized person is prohibited by law.

NOTICE
This document should not be returned after it has satisfied your requirements. It may be disposed of in accordance with your local security regulations or the appropriate provisions of the Industrial Security Manual for Safe-Guarding Classified Information.

CLASSIFIED BY ET DDr (10/3/72) NASw-2431
SUBJECT TO GENERAL DECLASSIFICATION
SCHEDULE OF EXECUTIVE ORDER 11652.
AUTOMATICALLY DOWNGRADED AT
TWO-YEAR INTERVALS.
DECLASSIFIED ON DECEMBER 31, 1973

NATIONAL AERONAUTICS AND SPACE ADMINISTRATION

CONFIDENTIAL

[redacted]

LONGITUDINAL AERODYNAMIC CHARACTERISTICS OF THE APOLLO COMMAND MODULE AT A MACH NUMBER OF 20 AND DATA COMPARISONS OVER A WIDE MACH NUMBER-REYNOLDS NUMBER RANGE*

By Julius E. Harris
Langley Research Center

SUMMARY

An experimental investigation has been conducted to determine the static longitudinal aerodynamic characteristics of the Apollo command module. The tests were made in the Langley hotshot tunnel at a Mach number M_∞ of approximately 20 and a Reynolds number $R_{\infty,d}$, based on maximum body diameter, of 0.15×10^6 for angles of attack from 0^o to 60^o.

The trim point occurred at an angle of attack of 33.5^o. The trim lift-drag ratio was -0.511 with corresponding lift and drag coefficients of -0.502 and 0.982, respectively. The maximum lift-drag ratio was -0.676 and occurred at an angle of attack of 50^o. Corresponding values of the lift and drag coefficients for the maximum lift-drag ratio were -0.396 and 0.586, respectively. The maximum lift coefficient was -0.505 and occurred at an angle of attack of 35^o. Estimates of the force and moment coefficients obtained from modified Newtonian impact theory agreed to within ±3 percent of the experimental results over the entire angle-of-attack range.

Analysis of the experimental results from the present investigation and comparisons with experimental data from previous investigations over a wide range of Mach numbers and Reynolds numbers $\left(3.3 \leqq M_\infty \leqq 20;\ 0.032 \times 10^6 \leqq R_{\infty,d} \leqq 2.430 \times 10^6\right)$ indicated that the variation in lift-drag ratio was a function of the shear force on the heat shield (forebody) and the pressure distribution in the separated region of the afterbody. The slope of the curve for the variation of lift coefficient with angle of attack at zero angle of attack $\left(C_{L_\alpha}\right)_{\alpha=0}$ was found to be a function of the shear stress on the blunt forebody. Both lift-drag ratio L/D and lift-curve slope $\left(C_{L_\alpha}\right)_{\alpha=0}$ were found to be logarithmic functions of the parameter $M_\infty/\sqrt{R_{\infty,d}}$ over the range of the Mach numbers and Reynolds numbers considered.

---

*Title, Unclassified.

[redacted]

INTRODUCTION

In order to determine the reentry trajectory for the Apollo command module, the aerodynamic characteristics must be accurately known as a function of both Reynolds number and Mach number since these parameters vary over a broad range during reentry. (See ref. 1.) It is not possible to obtain in existing ground test facilities all possible combinations of Mach number and Reynolds number that will occur during the actual reentry of the Apollo command module. Consequently, it is necessary to obtain data over as broad a range of Mach numbers and Reynolds numbers as possible in order to formulate correlation rules which will allow ground test facility data to be extended to more realistic flight expectations.

Recent analytical studies have shown that at moderate angles of attack, the unbalanced shear force about the axis of symmetry on the front face (forebody) of a blunt lifting reentry vehicle can contribute significantly to the reduction of the lift-drag ratio at low Reynolds numbers. (See refs. 2 and 3.) Experimental pressure distribution studies have further shown that the flow separation over the afterbody and the resulting pressure in this separated region are strong functions of both Mach number and Reynolds number. (See refs. 4, 5, and 6.) This pressure also affects the aerodynamic characteristics and in particular the lift-drag ratio.

In order to define more clearly the aerodynamic characteristics of the Apollo command module at high Mach numbers, an experimental program was initiated in the Langley hotshot tunnel to test a 0.019-scale model of the Apollo command module at a Mach number and Reynolds number of approximately 20 and 0.15×10^6, respectively, for angles of attack from 0^o to 60^o.

The results of this investigation are presented along with results from previous experimental investigations for comparison over the Mach number and Reynolds number range of 3.3 to 20 and 0.032×10^6 to 2.43×10^6, respectively.

SYMBOLS

The sign convention for the aerodynamic coefficients, the moment reference center location, and the body axis system used are presented in figure 1. The reference area and length for the force and moment coefficients are S and d, respectively.

a_∞ free-stream speed of sound, $\sqrt{\gamma_\infty p_\infty / \rho_\infty}$

C_A axial-force coefficient

C_D	drag coefficient
C_L	lift coefficient
$(C_{L\alpha})_{\alpha=0}$	slope of curve for variation of C_L with α evaluated at $\alpha = 0^o$
C_m	pitching-moment coefficient
$(C_{m\alpha})_{trim}$	slope of curve for variation of C_m with α evaluated at trim
C_N	normal-force coefficient
$(C_{N\alpha})_{\alpha=0}$	slope of curve for variation of C_N with α evaluated at $\alpha = 0^o$
$C_{p,max}$	maximum pressure coefficient, $\frac{\gamma + 3}{\gamma + 1}\left[1 - \frac{2}{M_\infty{}^2(\gamma + 3)}\right]$
d	maximum body diameter (see fig. 1)
L/D	lift-drag ratio
M_∞	free-stream Mach number, V_∞/a_∞
p_∞	free-stream static pressure
$p_{t,\infty}$	free-stream total pressure
$R_{\infty,d}$	Reynolds number, $\rho_\infty V_\infty d/\mu_\infty$
S	reference area, $\pi d^2/4$
T_∞	free-stream static temperature
$T_{t,\infty}$	free-stream total temperature
V_∞	free-stream velocity
x,z	body axis system (see fig. 1)
α	angle of attack

γ ratio of free-stream specific heats

μ_∞ coefficient of viscosity evaluated at free-stream temperature

ρ_∞ free-stream density

APPARATUS AND TESTS

Test Facility and Instrumentation

The present investigation was conducted at the Langley Research Center in the Langley hotshot tunnel. The Langley hotshot tunnel is a hypervelocity, arc-heated, blowdown facility. The major components of this facility include a capacitor bank with an electrical charging unit, an arc chamber incorporating coaxial electrodes, a 10° total-divergence-angle conical nozzle and test section followed by a 24-inch-diameter (0.61 m) cylindrical section, a 10° cone-cylinder diffuser, and a 300-cubic-foot (8.49 m^3) vacuum reservoir with vacuum pumps. The reader interested in the operation and calibration of this facility is referred to reference 7.

A three-component internally mounted strain-gage balance was used to measure the aerodynamic forces and moments exerted on the model during the investigation. The strain-gage outputs were amplified by a 3-kilocycle carrier amplifier system and recorded on an oscillograph. The total pressure in the arc chamber was measured with a strain-gage pressure transducer. This pressure, together with the initial arc-chamber density prior to arc discharge, was used to calculate the total temperature in the arc chamber. Pitot pressure in the test section was measured with a variable-reluctance transducer. This pressure, together with the arc-chamber conditions of total temperature and pressure, was used to calculate the free-stream thermodynamic properties.

Test Conditions and Data Accuracy

The approximate test conditions for the present investigation are as follows:

M_∞	20
$R_{\infty,d}$	0.15×10^6
$p_{t,\infty}$, N/m^2	7.58×10^7
$T_{t,\infty}$, $^\circ K$	3.00×10^3
p_∞, N/m^2	13.79
T_∞, $^\circ K$	48
Angle-of-attack range	$0^\circ \leq \alpha \leq 60^\circ$
Test gas ($\gamma = 1.4$)	Nitrogen

The maximum anticipated uncertainties in the force and moment coefficient data resulting from any error in the strain-gage-balance measurements, the carrier amplifier outputs, and the pitot-pressure measurements are:

C_N	±0.01
C_A	±0.01
C_m	±0.001

Models

The configuration used in the present investigation was a 0.019-scale model of the Apollo command module. Sectional views of the two test models are presented in figure 2. Two model-sting arrangements were used in an effort to minimize the effect of sting interference on the experimental force and moment data. (See ref. 8.) The center line of the balance was coincident with the model axis of symmetry for model 1 whereas it was inclined 27.5° to the axis of symmetry for model 2. Data were obtained with model 1 for $0^\circ \leqq \alpha \leqq 35^\circ$ and with model 2 for $20^\circ \leqq \alpha \leqq 60^\circ$. No discontinuities in the force and moment coefficient data were observed (as will be shown later) in the four-data-point overlap region, $20^\circ \leqq \alpha \leqq 35^\circ$. The models were machined from magnesium to minimize their weight and thus maximize balance response. A thin-wall 0.010-inch-thick (0.025 cm) 347 stainless-steel liner was pressed into the model balance can to insure a lasting fit between the balance and model since magnesium readily corrodes when exposed to air. The models each weighed approximately 0.08 pound (36.3 grams).

PRESENTATION OF RESULTS

Schlieren photographs for $0^\circ \leqq \alpha \leqq 60^\circ$ are presented in figure 3. The total-pressure probe used to measure the pitot pressure in the test section is visible in these photographs. This probe was located in a position such that no interference occurred between its flow field and that of the test model. A summary plot of the experimental shock-wave coordinates for angles of attack of 0°, 20°, 40°, and 60° is presented in figure 4. The static longitudinal aerodynamic characteristics obtained during the present investigation are presented in figure 5. Comparisons of static longitudinal aerodynamic characteristics over a wide range of Mach numbers and Reynolds numbers, $3.3 \leqq M_\infty \leqq 20$, $0.032 \times 10^6 \leqq R_{\infty,d} \leqq 2.43 \times 10^6$, are presented in figure 6. Correlations of the lift-drag-ratio data and the values the initial lift-coefficient slope evaluated at $\alpha = 0^\circ$ are presented in figures 7 and 8, respectively.

DISCUSSION

Basic Data

The static longitudinal aerodynamic characteristics obtained during the present investigation are presented in figure 5. Estimates of these characteristics using modified Newtonian impact theory are also presented. The values of $(C_{N_\alpha})_{\alpha=0}$ and $(C_{L_\alpha})_{\alpha=0}$ were approximately 0.0049 deg^{-1} and -0.023 deg^{-1}, respectively. The trim point occurred at $\alpha = 33.5^o$, $(C_{m_\alpha})_{trim}$ being approximately -0.0023 deg^{-1}. The trim lift-drag ratio was -0.511 with corresponding values of C_L and C_D of -0.502 and 0.982, respectively. (See figs. 5(b) and 5(c).) Maximum L/D occurred at $\alpha = 50^o$ and was -0.676. The values of C_L and C_D corresponding to maximum L/D were -0.396 and 0.586, respectively. The maximum lift coefficient was -0.505 and occurred at an angle of attack of 35^o.

Estimates of the force and moment coefficient using modified Newtonian impact theory, $C_{p,max} = 1.832$ agreed well with the experimental data from the present investigation over the entire angle-of-attack range. In most instances the actual magnitudes of the coefficients were predicted within ±3 percent.

Comparisons and Correlations

Before proceeding further with the discussion of the experimental results, it is important that two important factors which may affect the aerodynamic characteristics of the Apollo command module be discussed in order to understand more clearly the data presented in subsequent figures.

The Apollo vehicle enters the atmosphere at some nonzero angle of attack; consequently, the flow stagnation point is not coincident with the geometric stagnation point ($x = z = 0$). This nonzero angle of attack produces flow asymmetries on the forebody such that the integrated shear force does not balance out about the vehicle center line (X-axis). This unbalanced shear force, depending on the value of Reynolds number, may produce a major reduction in lift, a minor addition to drag, and consequently a decrease in the lift-drag ratio. It was analytically shown in reference 3 that the forebody shear force on the Gemini reentry vehicle significantly reduced the lift and resulting lift-drag ratio at high altitudes. It was further concluded in reference 3 that for shock Reynolds numbers R_S less than 1×10^4, the viscous contributions to lift must be included. $(R_S = \rho_\infty V_\infty d/\mu_S$ where μ_S is the coefficient of viscosity behind the normal shock.) For example, their neglect at $R_S = 1 \times 10^2$ and $M_\infty = 25$ will result in errors of the order of 40 percent in the lift coefficient. (See ref. 3.) However, the results presented in references 2 and 3 do not consider the contribution of the afterbody to the resultant

lift and lift-drag ratio which should be considered when the effect of low Reynolds number on the actual reentry vehicle is determined.

As the Reynolds number becomes small $\left(R_S < 1 \times 10^4\right)$, the shear force on the conical afterbody of the Apollo command module may also affect the resultant lift-drag ratio. Oil-flow photographs presented in figure 9 of reference 4 for angles of attack of 35^o and 55^o allow a qualitative assessment of the effect on the aerodynamic characteristics of the Apollo command module of the integrated shear force over the afterbody. At $\alpha = 35^o$ in the region of the most windward ray, the streamlines are alined nearly parallel to the free stream with the result that in this high shear stress region the contribution is primarily to drag. However, as the streamlines proceed around the afterbody toward the separation point, the shear stress not only contributes to drag but also decreases the lift. Consequently, the shear force on the afterbody, in general, tends to reduce the lift, increase the drag, and thus reduce the resultant lift-drag ratio.

In references 5 and 6 it was shown that the pressure in the separated region of the afterbody was a function of both Mach number and Reynolds number. The pressure coefficient in this region was observed to increase with both increasing Mach number and decreasing Reynolds number. For example, at zero angle of attack, it was shown in reference 6 that the pressure coefficient in the separated region increased from 0.014 to 0.032 for a Mach number increase from 10 to 20. At small angles of attack near $\alpha = 0^o$ where the separation is nearly symmetrical around the afterbody, the resultant effect would be to increase the lift-drag ratio by decreasing the resultant drag. At positive angles of attack the separation would become nonsymmetrical (see ref. 4) and would not only decrease the drag but also increase the lift. Consequently, the pressure in the separated region would tend to oppose the effect of the viscous shear force at low Reynolds numbers and high Mach numbers.

Experimental data from references 9 and 10, data obtained from North American Aviation, Inc., under Contract NAS9-150, and the data obtained in the present investigation are presented in figure 6. These data cover a Mach number and Reynolds number range of 3.3 to 20 and 0.032×10^6 to 2.43×10^6, respectively, for angles of attack from 0^o to 60^o.

The spread in the C_N data from the various references is fairly consistent over the entire angle-of-attack range (see fig. 6(a)); whereas the spread in the C_A data is greatest near $\alpha = 0^o$ and decreases as α increases. The C_A datum point at $\alpha = 0^o$ from the present investigation is approximately 9 percent higher than the mean value of 1.46 as established by the previous investigations. One possible explanation for this disagreement is the previously mentioned contribution of the pressure in the separated region which reduces C_A. In the Langley hotshot tunnel (see ref. 6), it was found that the flow separated further rearward than at lower Mach number tests. Consequently,

the pressure in the separated region acts over a smaller surface area and as such, decreases the C_A less than at lower Mach numbers where separation occurs at the shoulder. (See ref. 4.) Within the accuracy of the C_m data, the results from all the investigations agreed well on the trim angle of attack as well as on $(C_{m_\alpha})_{trim}$. Little, if any, data scatter occurred throughout the angle-of-attack range. (See fig. 6(b).) This agreement over the range $0^o \leqq \alpha \leqq 60^o$ for the various investigations is probably due to a compensating effect between the combined forebody-afterbody shear force and the separated pressure force contributions to pitch about the moment reference center.

The agreement between the C_L data is reasonably good over the entire α range with exception of that from reference 10. (See fig. 6(c).) However, careful attention should be given to the differences in C_D for $0 \leqq \alpha \leqq \alpha_{trim}$. It appears from these data points that any differences in the resultant lift-drag ratio are not necessarily due to lift contributions as previously mentioned, but in fact could possibly be attributed to variations of drag. As previously mentioned, the factor which contributes primarily to drag force reduction is the pressure in the separated region and not the shear stress on the forebody.

From the data presented in figure 6(d) it appears that the maximum lift-drag ratio occurs at an angle of attack of approximately 50^o. Particular attention should be given to the order of the symbols at $\alpha = 50^o$. That is, with the exception of the data point from reference 10, $(L/D)_{max}$ decreases with increasing Reynolds number and with decreasing Mach number. Note also the apparent discontinuity in the slope of the data from reference 10 in the interval $20^o \leqq \alpha \leqq 30^o$. This discontinuity may be attributed to sting interference. Consequently, data from reference 10 for $\alpha > 20^o$ are omitted from subsequent figures.

A more thorough study of the lift-drag ratio can be made from figure 7. Data are plotted as functions of the parameter $M_\infty/\sqrt{R_{\infty,d}}$ for angles of attack of 10^o, 20^o, 30^o, and 40^o. The parameter $M_\infty/\sqrt{R_{\infty,d}}$ was previously used in reference 11 to correlate the L/D characteristics of various reentry configurations. The lift-drag ratio L/D appears to be a logarithmic function of $M_\infty/\sqrt{R_{\infty,d}}$. Of particular interest is the trend of the variation of L/D with $M_\infty/\sqrt{R_{\infty,d}}$ with increasing α. For example, L/D decreases with increasing $M_\infty/\sqrt{R_{\infty,d}}$ for $\alpha < 30^o$, remains constant with increasing $M_\infty/\sqrt{R_{\infty,d}}$ for $\alpha = 30^o$, and increases with increasing $M_\infty/\sqrt{R_{\infty,d}}$ for $\alpha > 30^o$. The change in the trend of L/D with increasing $M_\infty/\sqrt{R_{\infty,d}}$ and α appears to occur just prior to the angle of attack for which the afterbody becomes exposed to the flow. Modified Newtonian theory estimates of the lift-drag ratio for angles of attack of 10^o, 20^o, 30^o, and 40^o are compared with the experimental data in figure 7. The agreement is good for $\alpha \leqq 20^o$; however, for $\alpha > 20^o$, the modified Newtonian values are somewhat greater than the experimental values.

The slope of the curve of lift coefficient plotted against angle of attack evaluated at $\alpha = 0^{\circ}$ is presented in figure 8(a) as a function of $M_{\infty}/\sqrt{R_{\infty,d}}$. The slope $(C_{L_{\alpha}})_{\alpha=0}$ decreases with increasing M_{∞} and decreasing $R_{\infty,d}$. (See figs. 8(b) and 8(c).) This trend can be attributed primarily to the unbalanced shear force about the point $x = z = 0$ on the forebody since, for a perturbation to α at $\alpha = 0^{\circ}$, the separation remains very nearly symmetrical about the afterbody and, as such, the pressure in this region contributes to negative drag only. Consequently, the data presented in figure 8 are in agreement with the trend of the analytical results presented in reference 3.

CONCLUSIONS

The results of an experimental investigation to determine the static longitudinal aerodynamic characteristics of a 0.019-scale model of the Apollo command module have been presented. The investigation was made in the Langley hotshot tunnel at a Mach number of approximately 20 and a Reynolds number, based on the maximum body diameter, of 0.15×10^6 for angles of attack from 0° to 60°.

An analysis of the data from the present investigation, together with comparisons of the results of previous investigations over the Mach number and Reynolds number range of 3.3 to 20 and 0.032×10^6 to 2.430×10^6, and comparisons with Newtonian theory has yielded the following conclusions.

1. The trim point occurred at an angle of attack of approximately 33.5° and appeared to be independent of both Mach number and Reynolds number. The trim lift-drag ratio was -0.511 and corresponding values of lift and drag coefficient were -0.502 and 0.982, respectively.

2. The maximum lift-drag ratio was -0.676 and occurred at an angle of attack of 50°. Corresponding values of lift and drag coefficients were -0.396 and 0.586, respectively. The maximum lift coefficient was -0.505 and occurred at an angle of attack of 35°.

3. The slope of the curve of the variation of lift coefficient with angle of attack evaluated at zero angle of attack $(C_{L_{\alpha}})_{\alpha=0}$ was found to be a function of the shear stress on the blunt forebody. Both lift-drag ratio L/D and $(C_{L_{\alpha}})_{\alpha=0}$ were found to be logarithmic functions of the parameter $M_{\infty}/\sqrt{R_{\infty,d}}$ over the range of Mach numbers M_{∞} and Reynolds numbers $R_{\infty,d}$ considered.

4. Estimates of the force and moment coefficients using modified Newtonian impact theory agreed with the trends of the experimental data over the entire angle-of-attack range and in most instances agreed with the actual magnitude within ±3 percent.

Langley Research Center,
National Aeronautics and Space Administration,
Langley Station, Hampton, Va., January 31, 1967,
124-07-02-54-23.

REFERENCES

1. Moseley, William C., Jr.; and Martino, Joseph C.: Apollo Wind Tunnel Testing Program – Historical Development of General Configurations. NASA TN D-3748, 1966.
2. Goldberg, Leon: Low Reynolds Number Effects on the Trajectory of a Blunt Lifting Reentry Vehicle. R65SD59, Missile and Space Div., Gen. Elec. Co., Nov. 1965.
3. Goldberg, Leon: Forces and Moments on the Front Face of a Blunt Lifting Reentry Vehicle. AIAA Paper No. 66-464, Am. Inst. Aeron. Astronaut., June 1966.
4. Jones, Robert A.: Experimental Investigation of the Overall Pressure Distribution, Flow Field, and Afterbody Heat-Transfer Distribution of an Apollo Reentry Configuration at a Mach Number of 8. NASA TM X-813, 1963.
5. Jones, Robert A.; and Hunt, James L.: Recent Experimental Studies on Heat Transfer to Apollo Command Module. NASA SP-101, 1965, pp. 9-18.
6. Miller, Charles G., III; and Lawing, Pierce L.: Experimental Investigation of Flow Characteristics of the Apollo Reentry Configuration at a Mach Number of 20 in Nitrogen. NASA TM X-1258, 1966.
7. Miller, Charles G., III; Creel, Theodore R., Jr.; and Smith, Fred M.: Calibration Experience in the Langley Hotshot Tunnel for Mach Numbers From 12 to 26. NASA TN D-3278, 1966.
8. Stivers, Louis S., Jr.: Effects of a Sting Support on the Supersonic Force and Moment Characteristics of an Apollo Model at Angles From -30° to $+185^{\circ}$. NASA TM X-1081, 1965.
9. Neal, Luther, Jr.: An Exploratory Investigation at a Mach Number of 6.9 Into the Use of Aerodynamic Controls for Modulating the Lift-Drag Ratio of an Apollo Type Configuration. NASA TM X-816, 1963.
10. Jorgensen, Leland H.; and Graham, Lawrence A.: Predicted and Measured Aerodynamic Characteristics for Two Types of Atmosphere-Entry Vehicles. NASA TM X-1103, 1965.
11. Boylan, D. E.; and Potter, J. L.: Aerodynamics of Typical Lifting Bodies Under Conditions Simulating Very High Altitudes. AIAA Paper No. 66-467, Am. Inst. Aeron. Astronaut., June 1966.

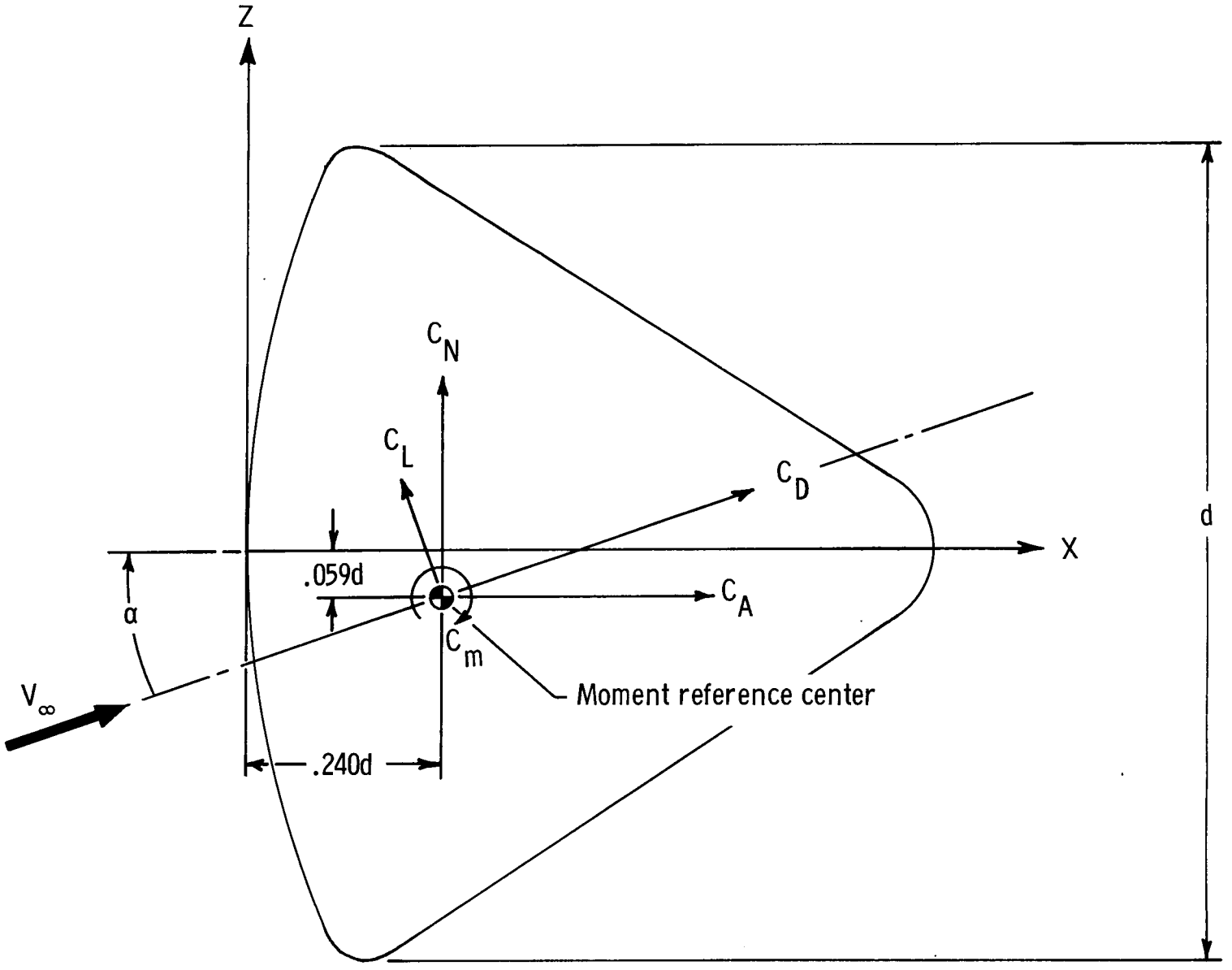

Figure 1.- Sign convention. Arrows indicate positive direction. d = 3.00 in. (7.62 cm).

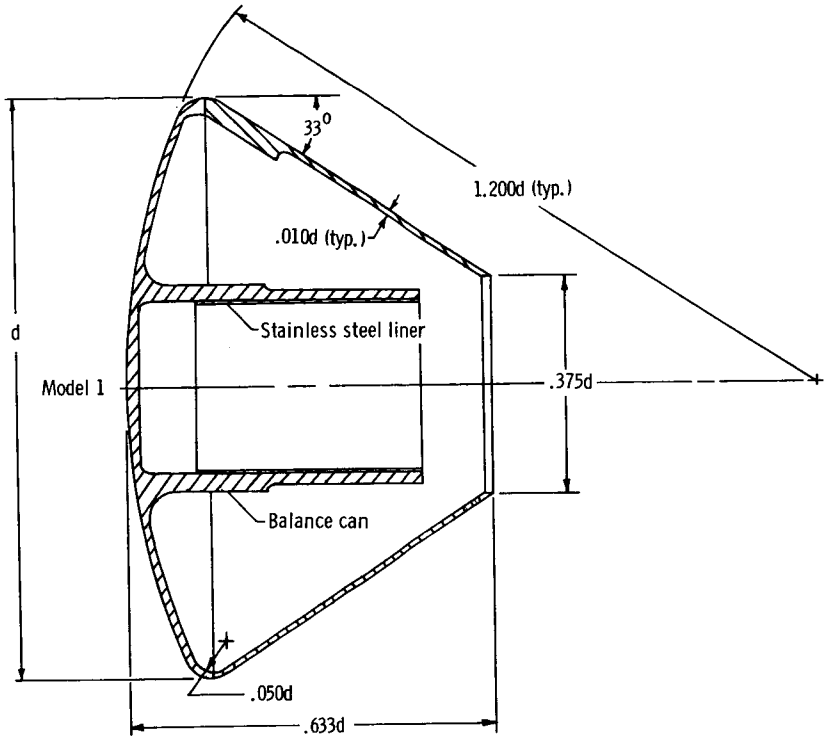

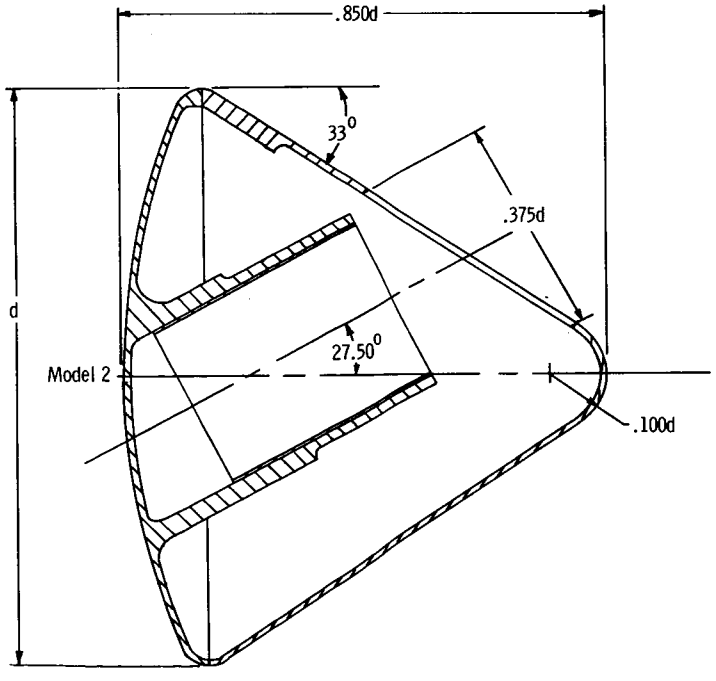

Figure 2.- Sectional view of models. d = 3.00 in. (7.62 cm).

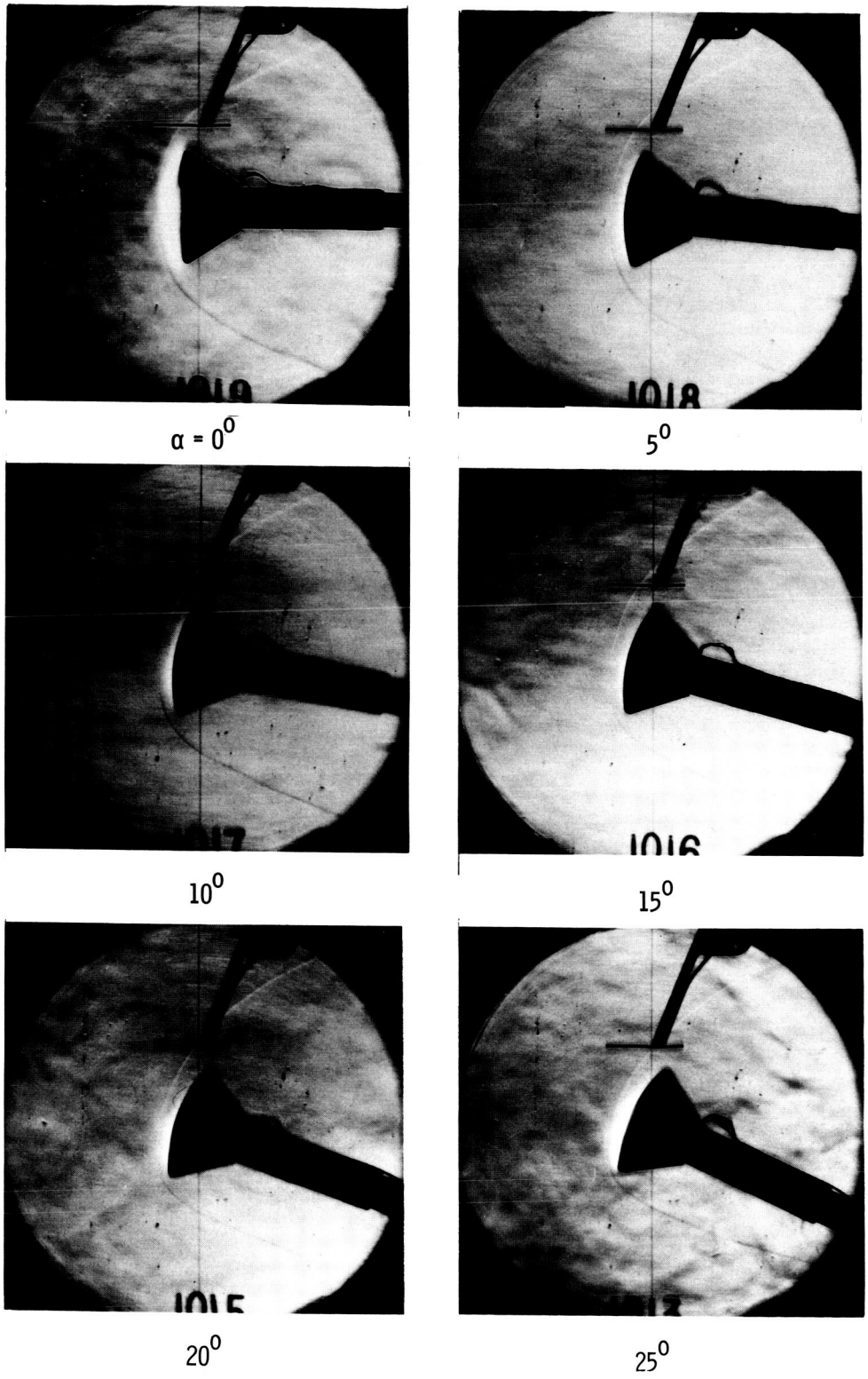

(a) $0^0 \leq \alpha \leq 25^0$. L-67-951

Figure 3.- Schlieren photographs. $M_\infty = 20$; $R_{\infty,d} = 0.15 \times 10^6$.

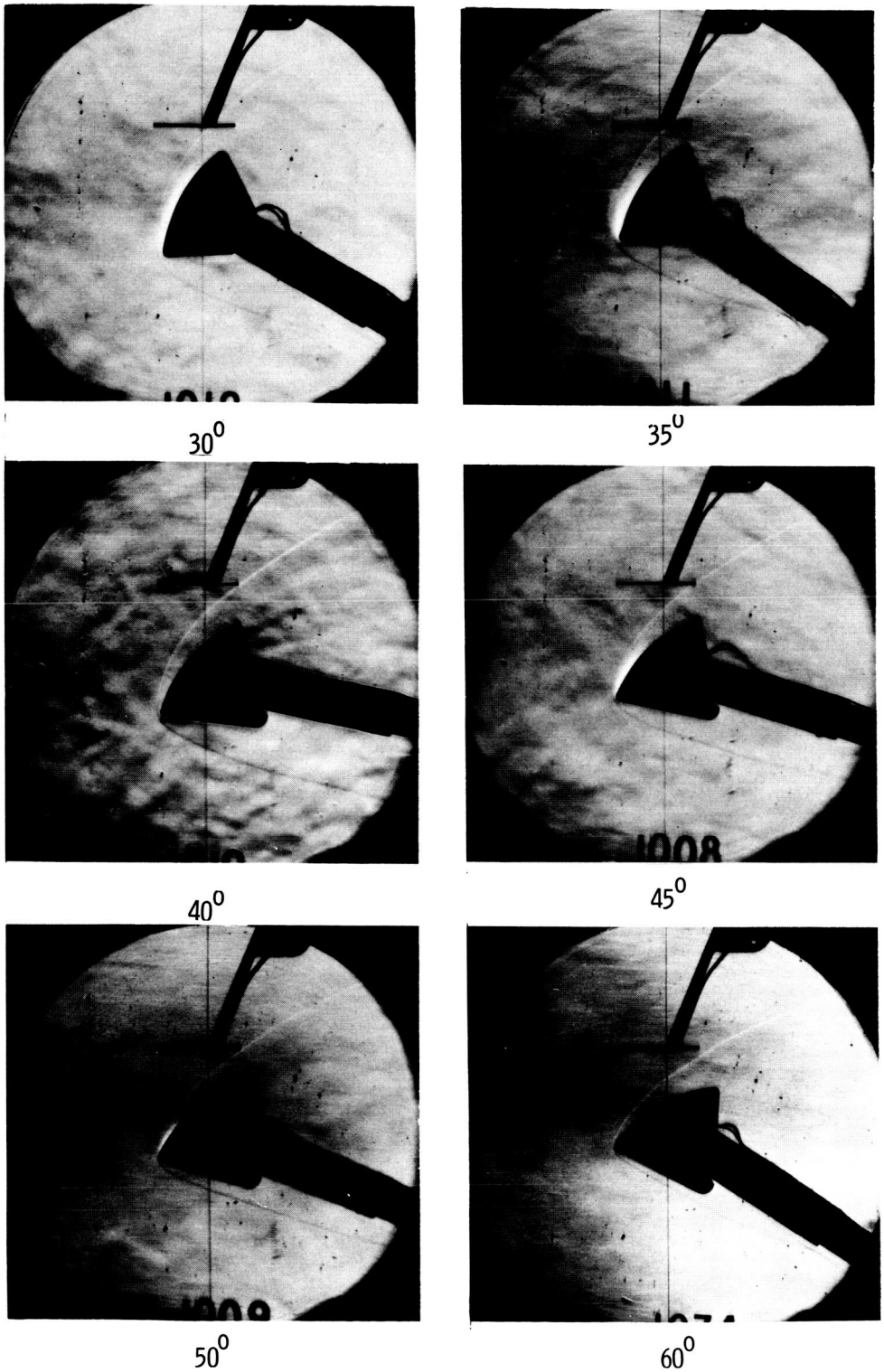

(b) $30^{\circ} \leq \alpha \leq 60^{\circ}$.

L-67-952

Figure 3.- Concluded.

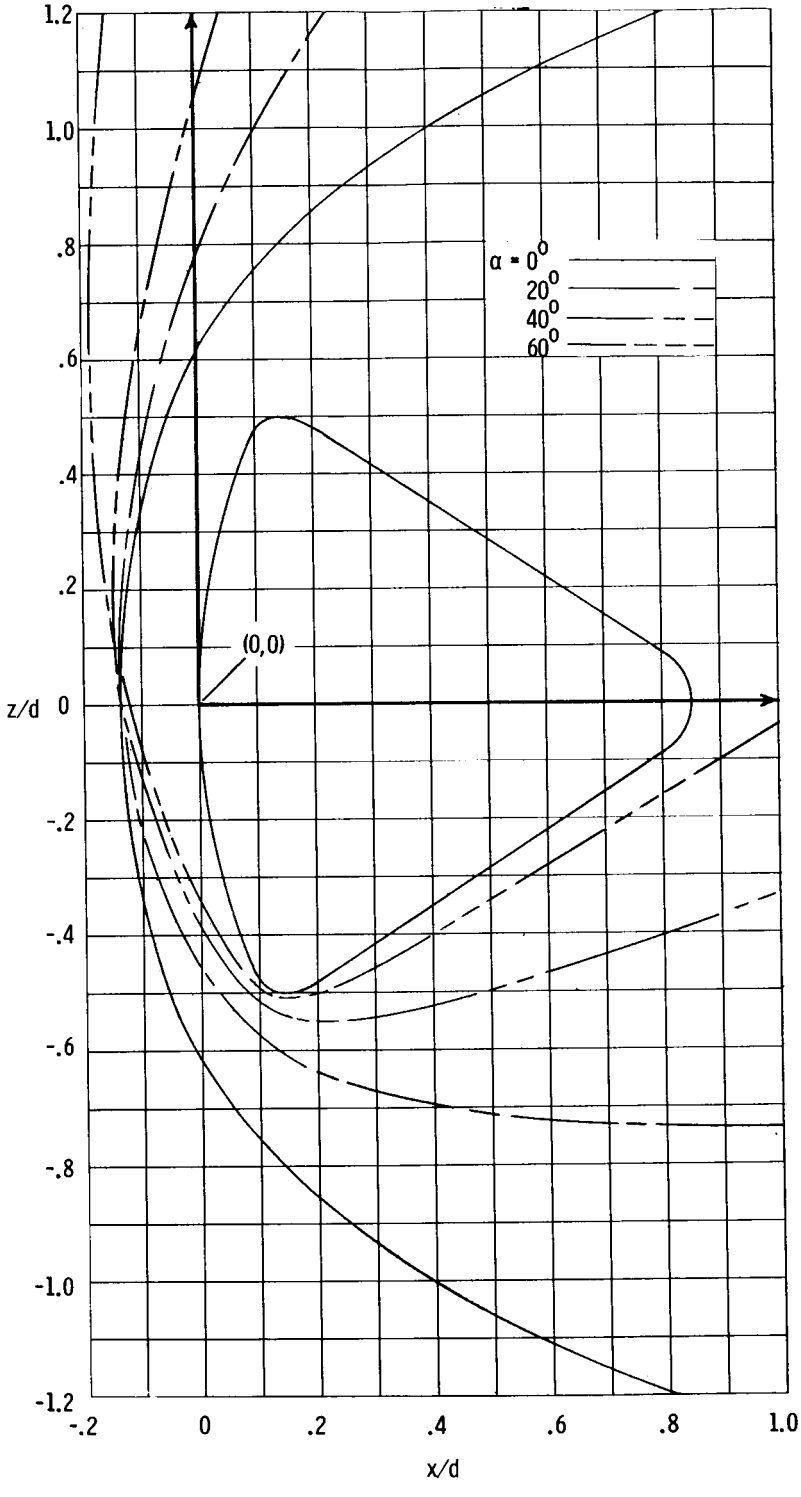

Figure 4.- Shock shapes. $M_\infty = 20$; $R_{\infty,d} = 0.15 \times 10^6$.

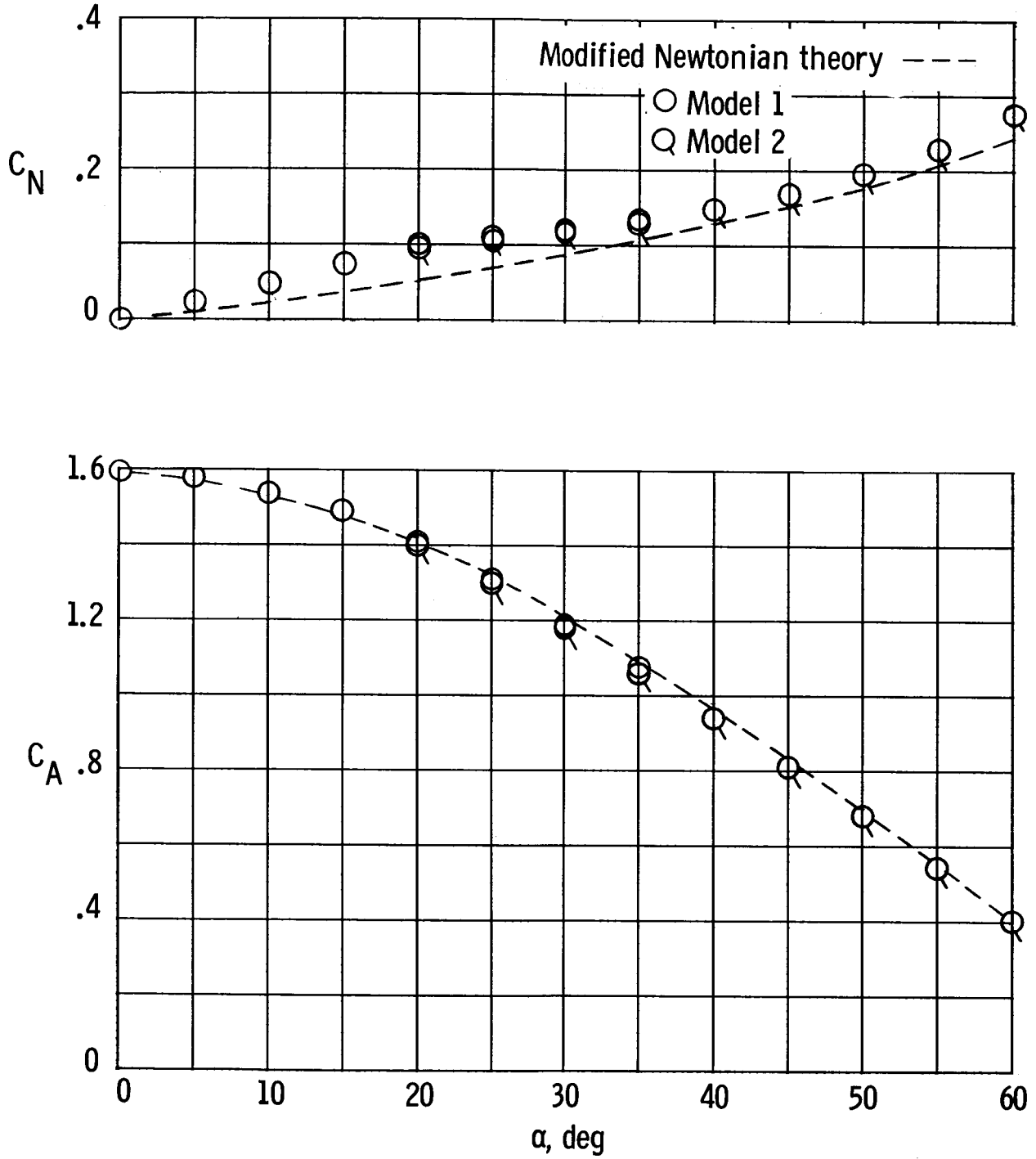

(a) Variation of C_N and C_A with α.

Figure 5.- Longitudinal aerodynamic characteristics. $M_\infty = 20$; $R_{\infty,d} = 0.15 \times 10^6$.

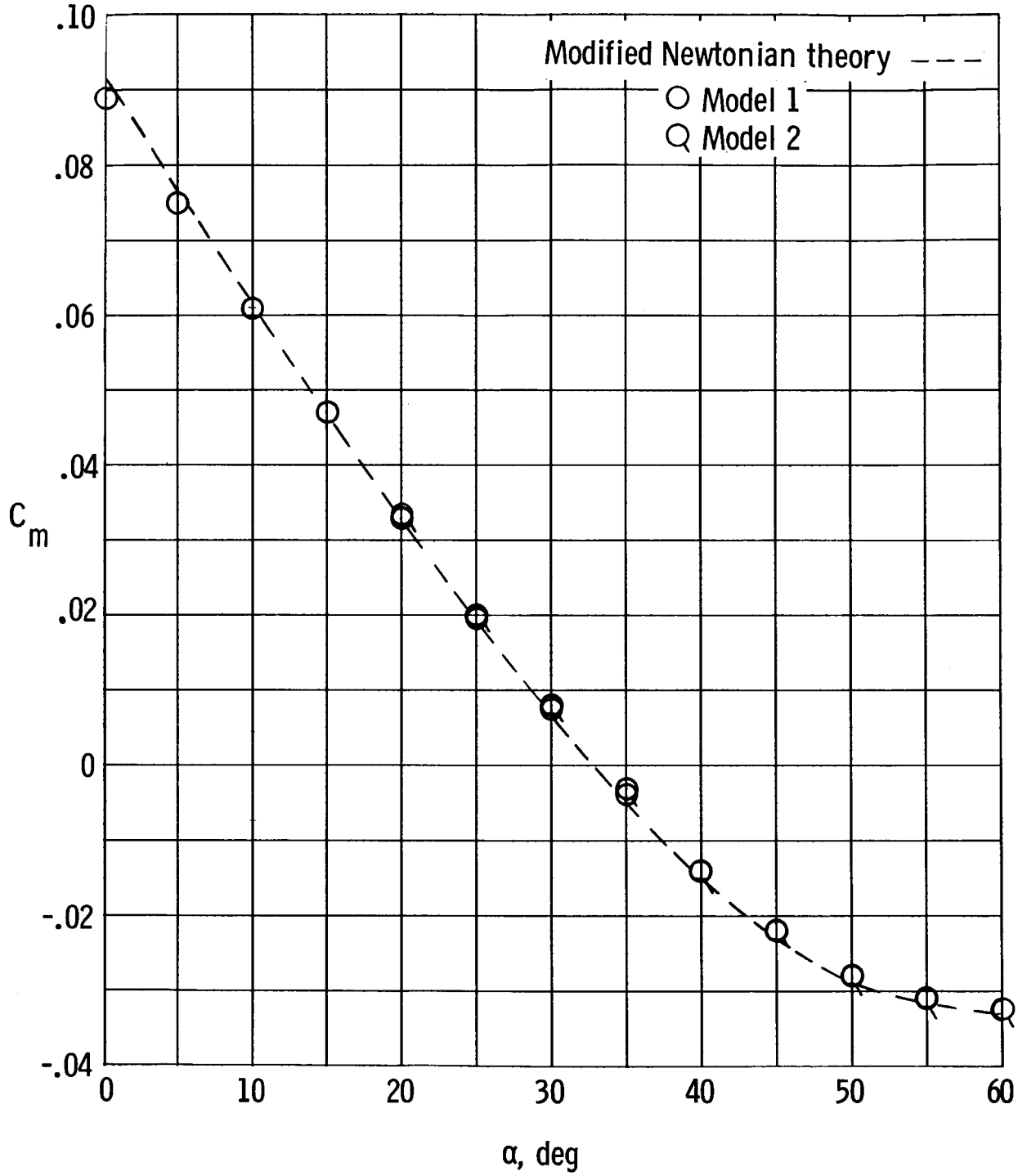

(b) Variation of C_m with α.

Figure 5.- Continued.

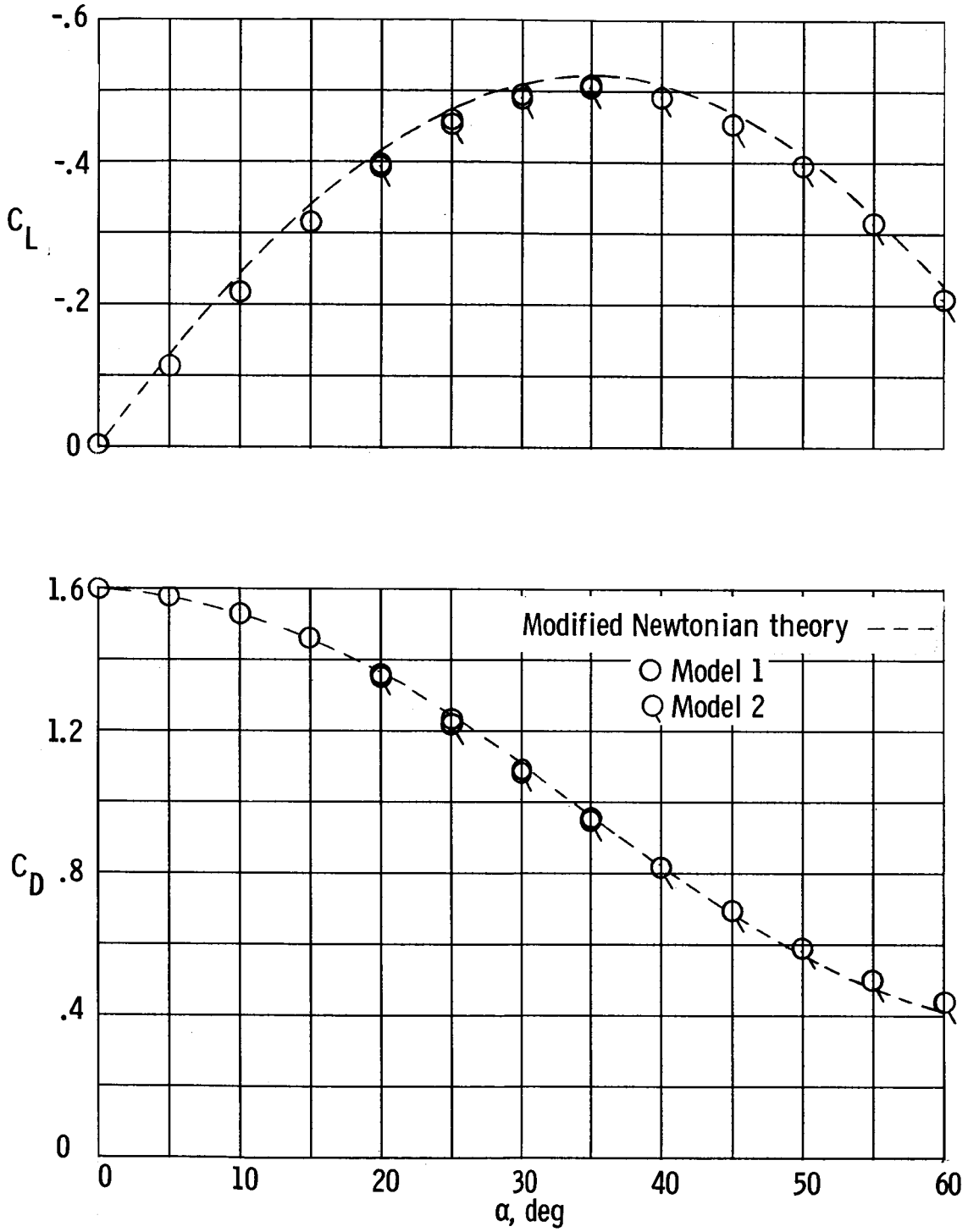

(c) Variation of C_L and C_D with α.

Figure 5.- Continued.

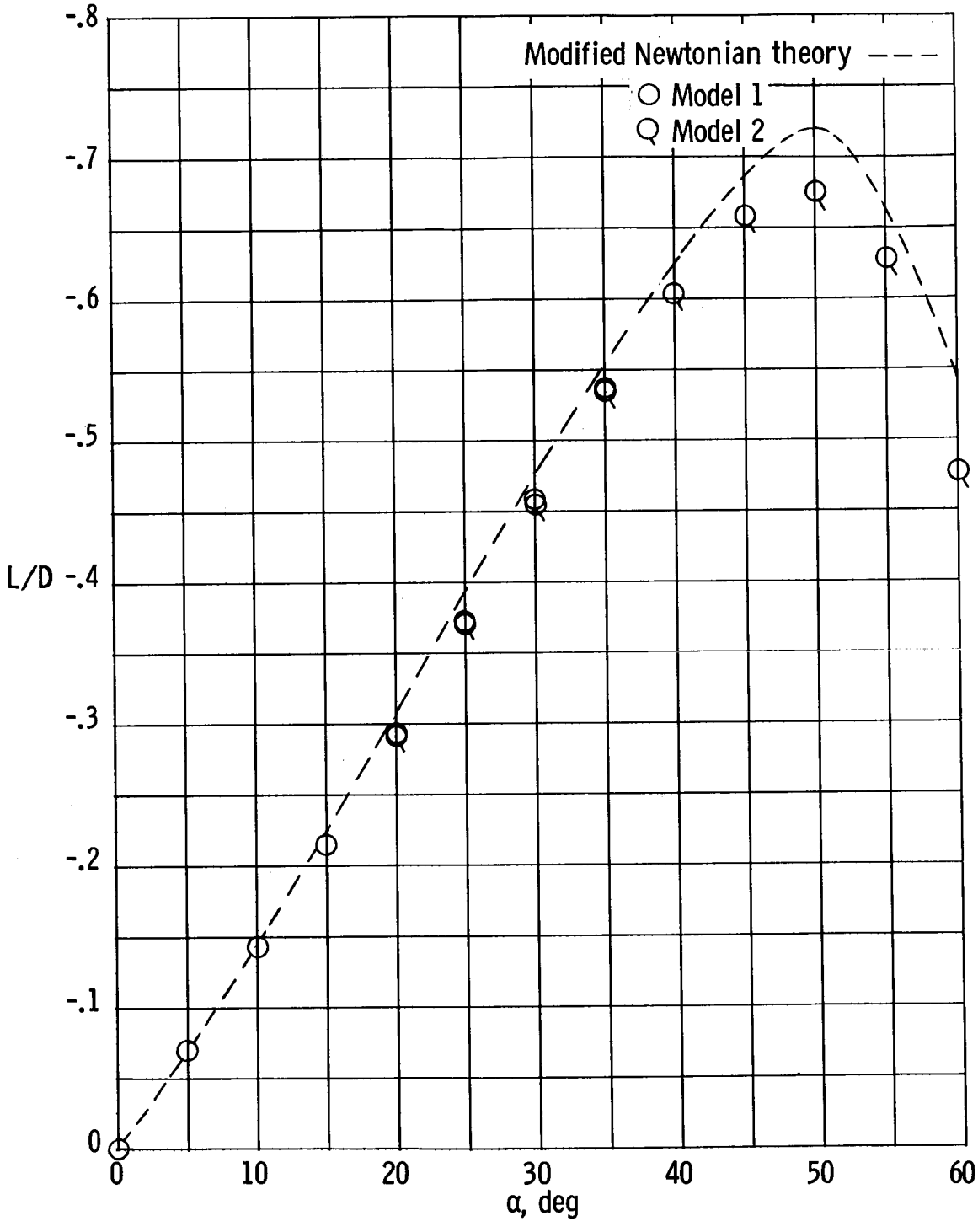

(d) Variation of L/D with α.

Figure 5.- Concluded.

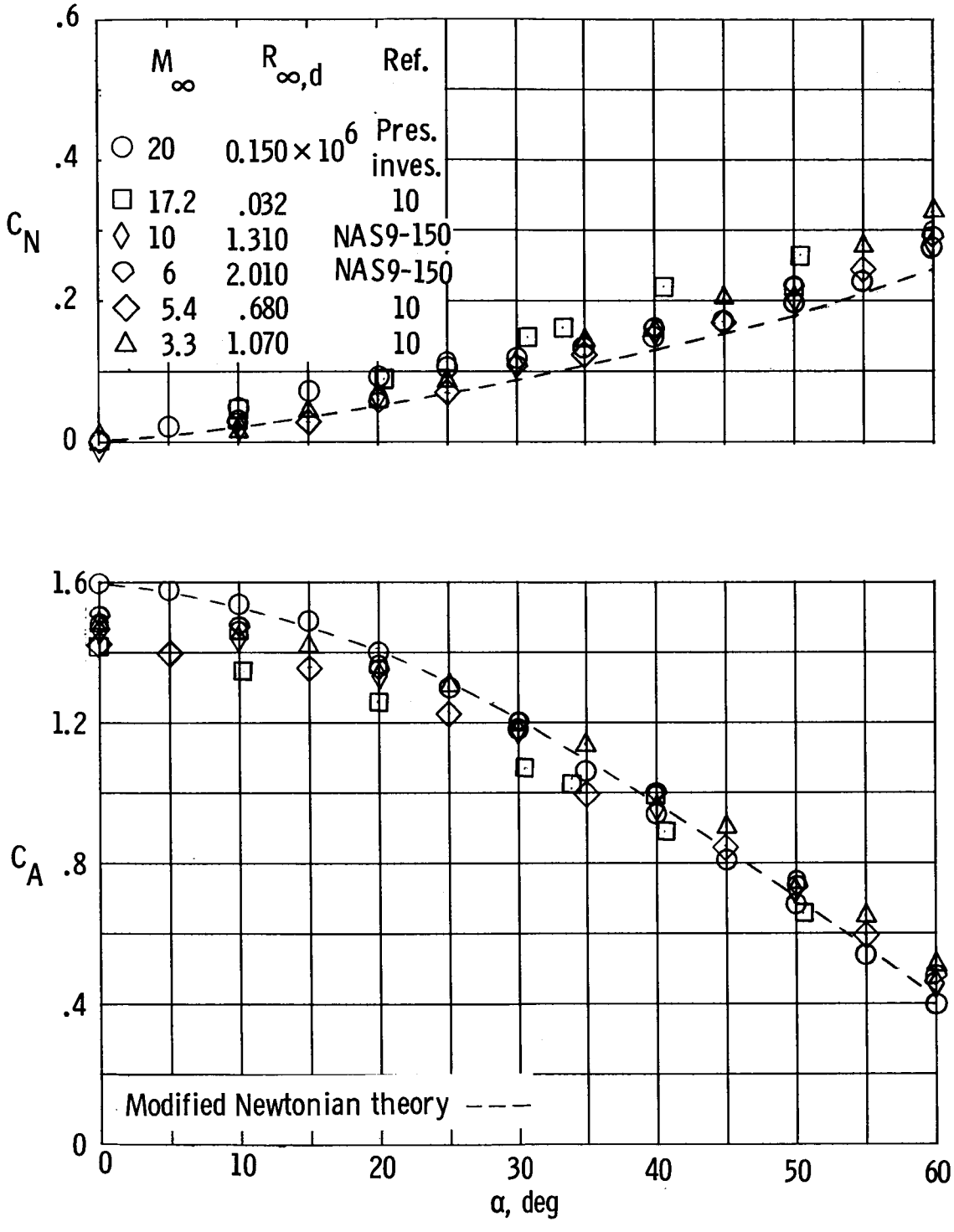

(a) Variation of C_N and C_A with α.

Figure 6.- Comparisons of longitudinal aerodynamic characteristics.

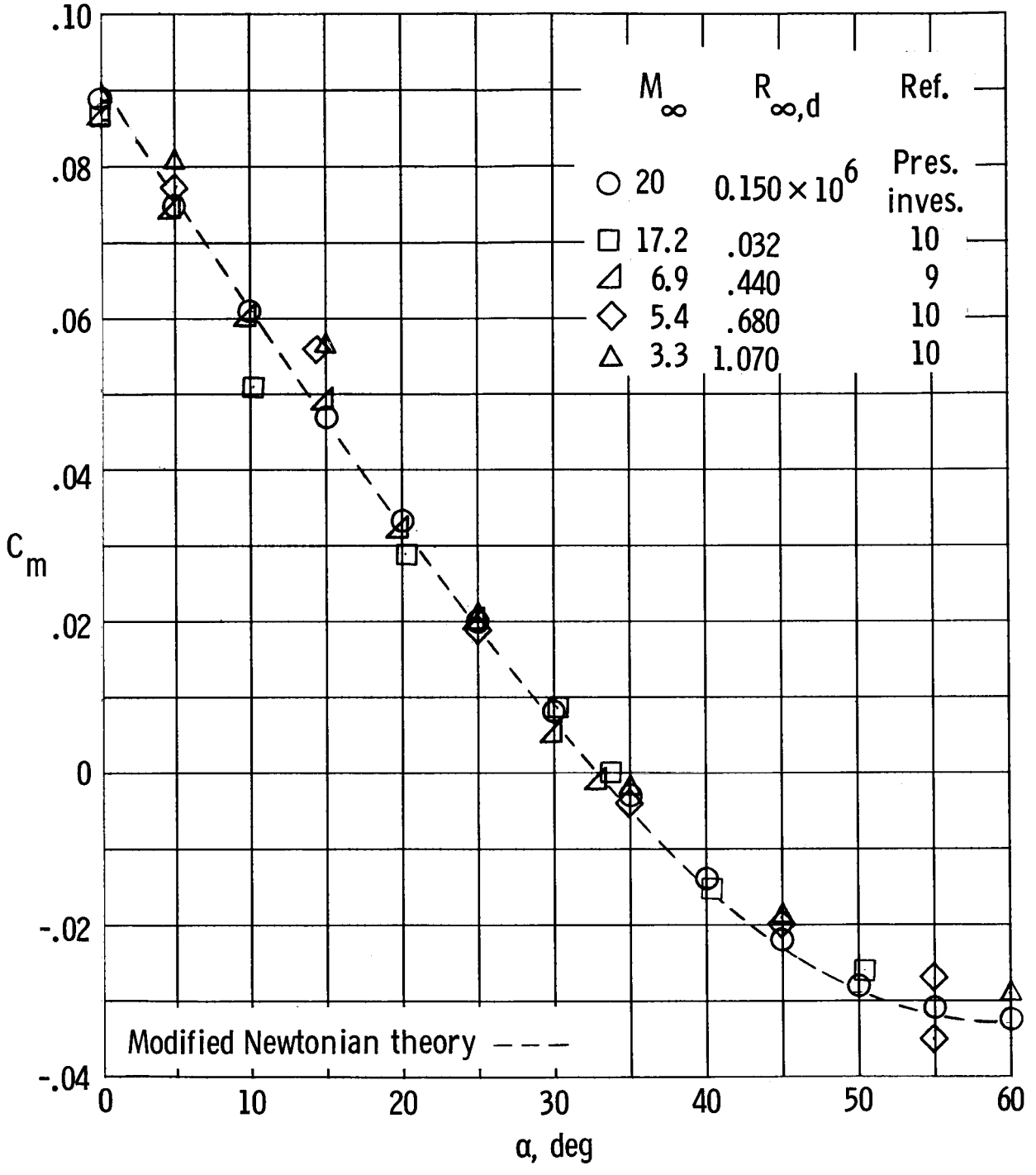

(b) Variation of C_m with α.

Figure 6.- Continued.

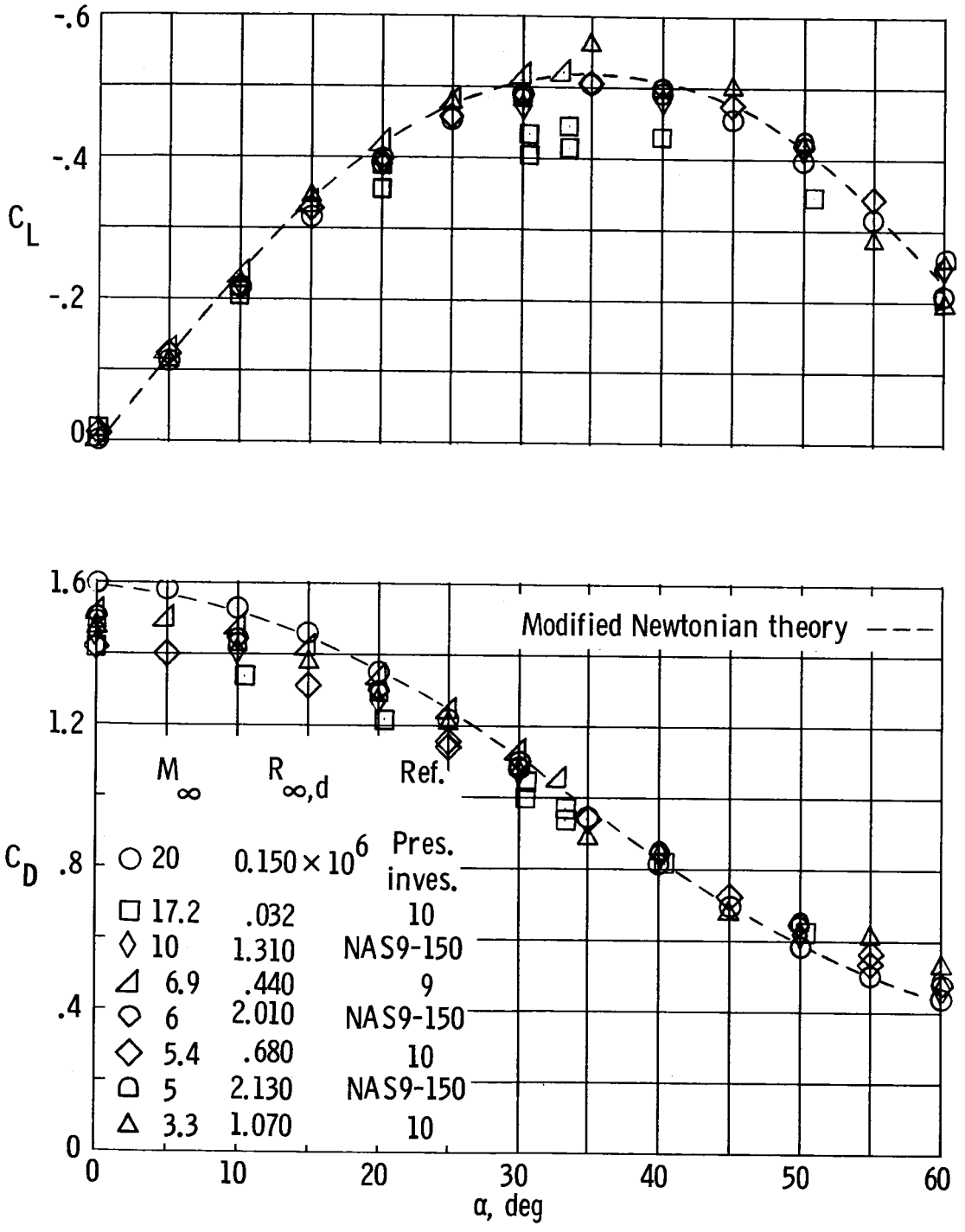

(c) Variation of C_L and C_D with α.

Figure 6.- Continued.

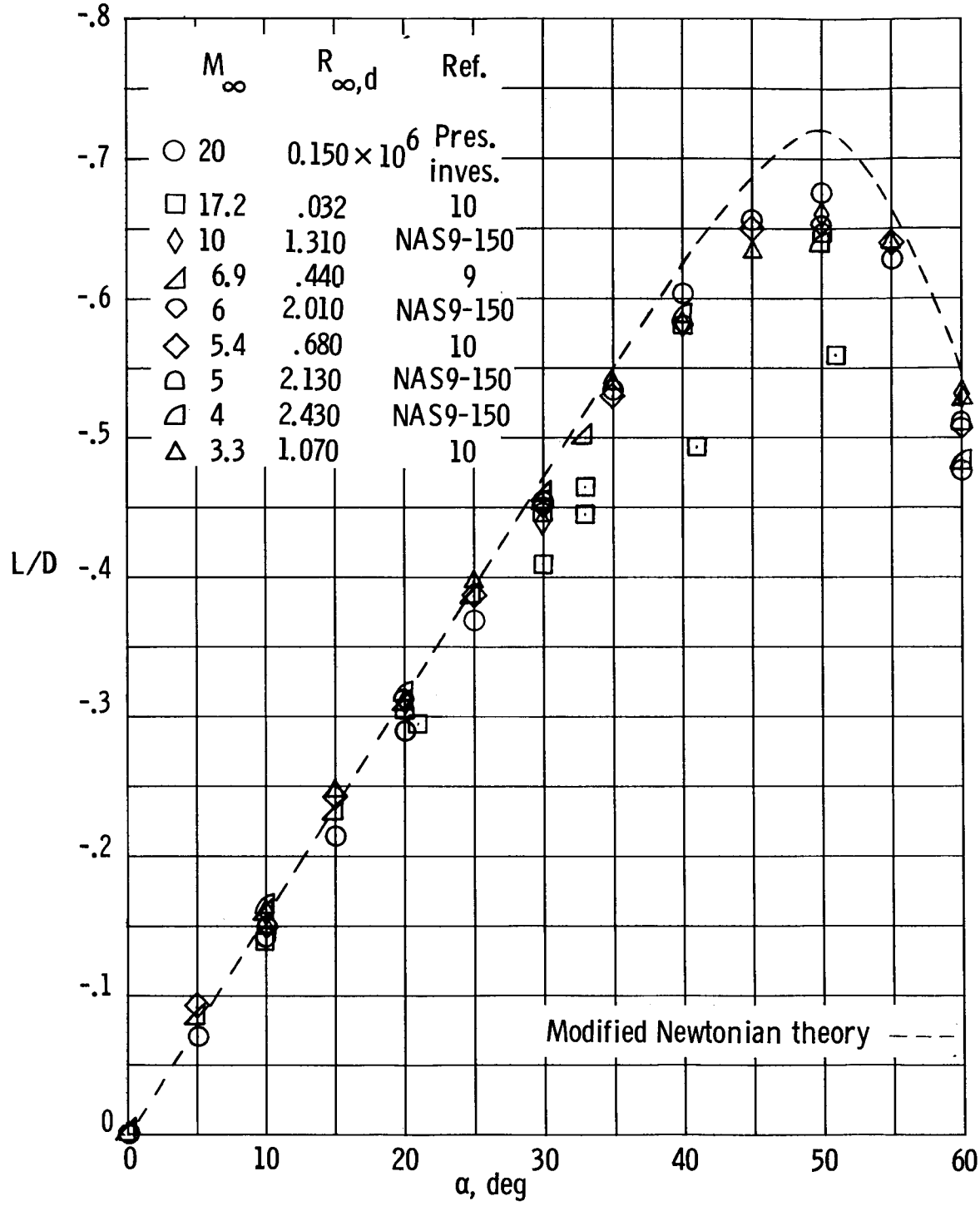

(d) Variation of L/D with α.

Figure 6.- Concluded.

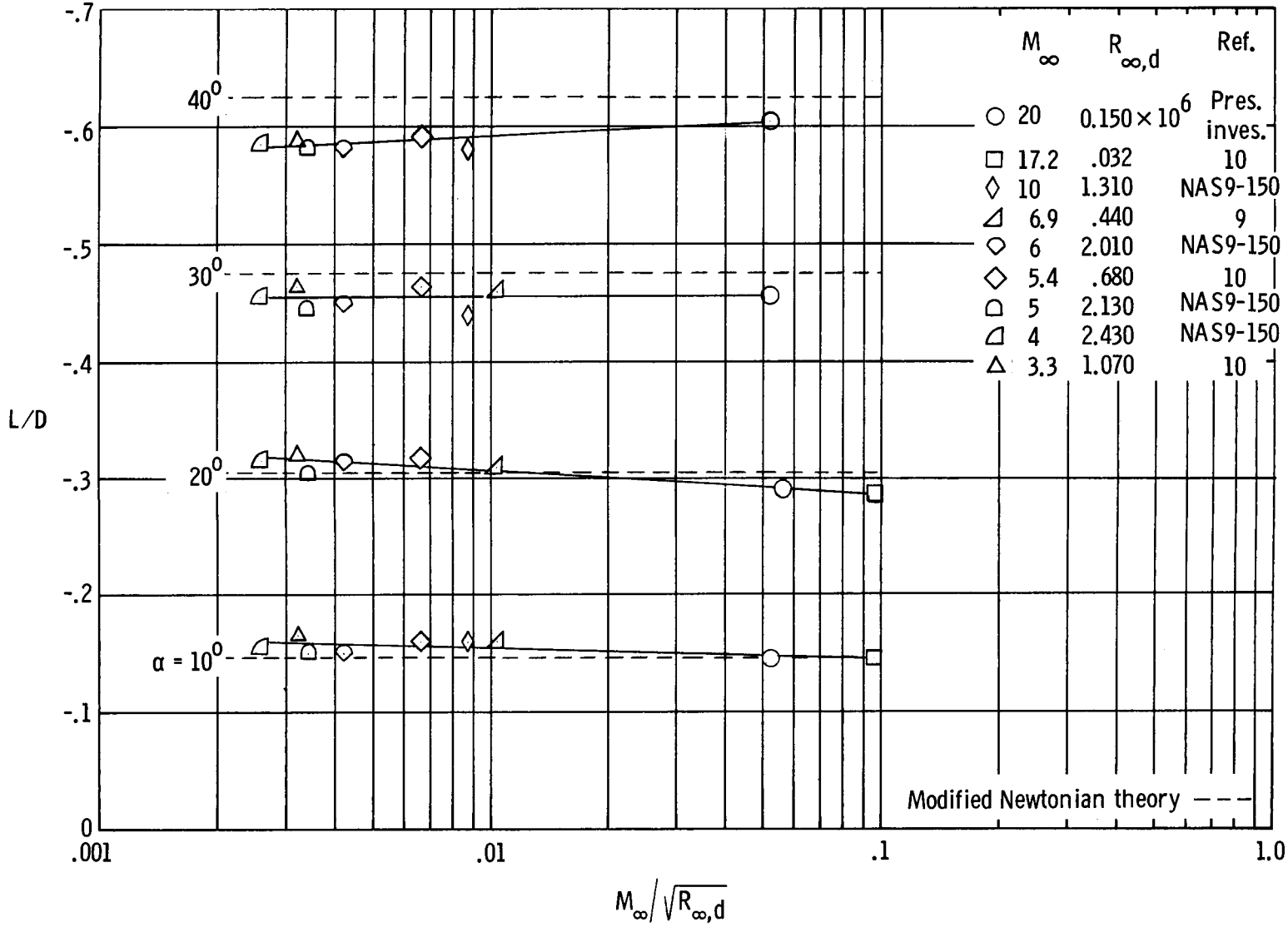

(a) Variation of L/D with $M_\infty/\sqrt{R_{\infty,d}}$.

Figure 7.- Lift-drag study.

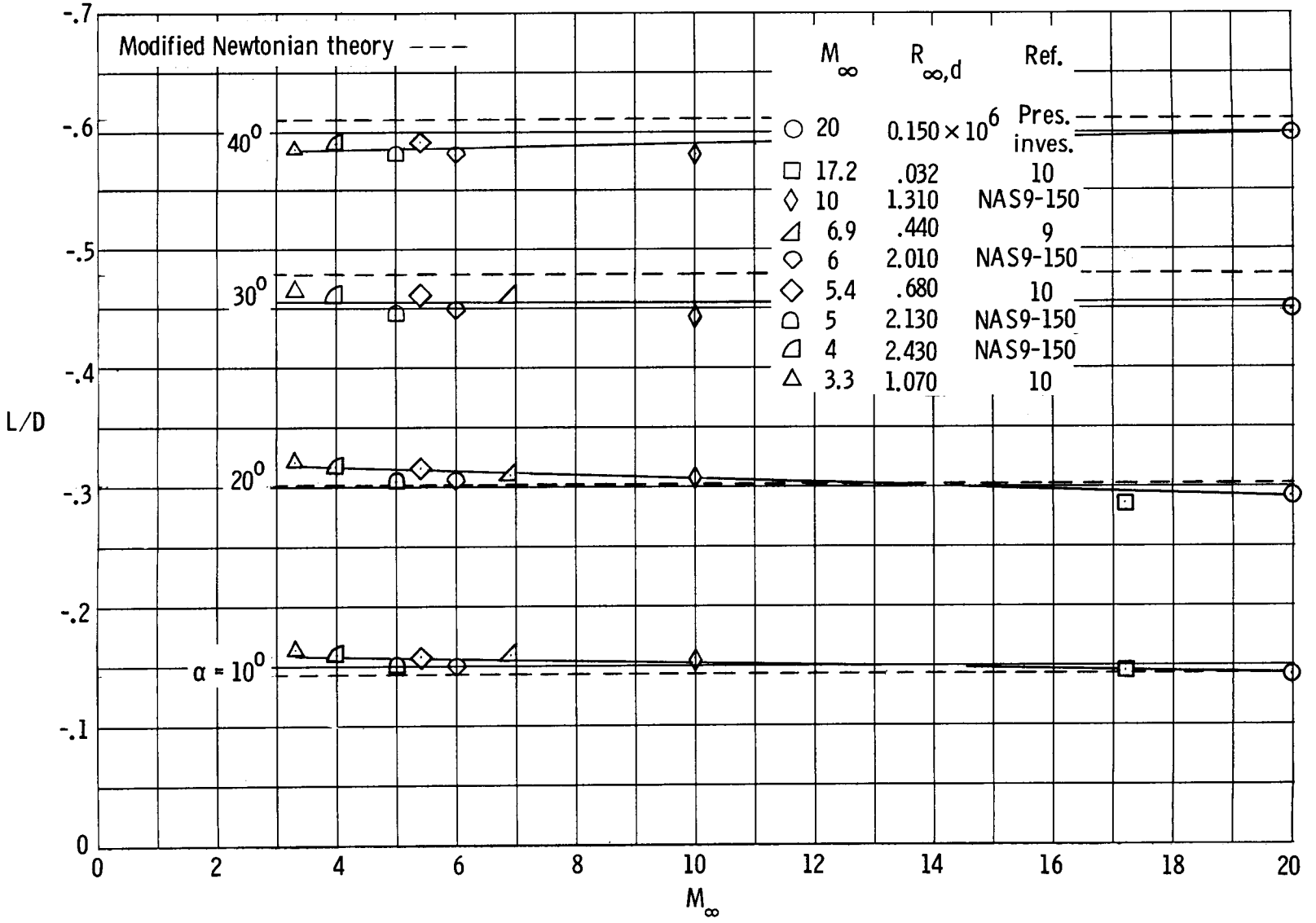

(b) Variation of L/D with M_∞.

Figure 7.- Continued.

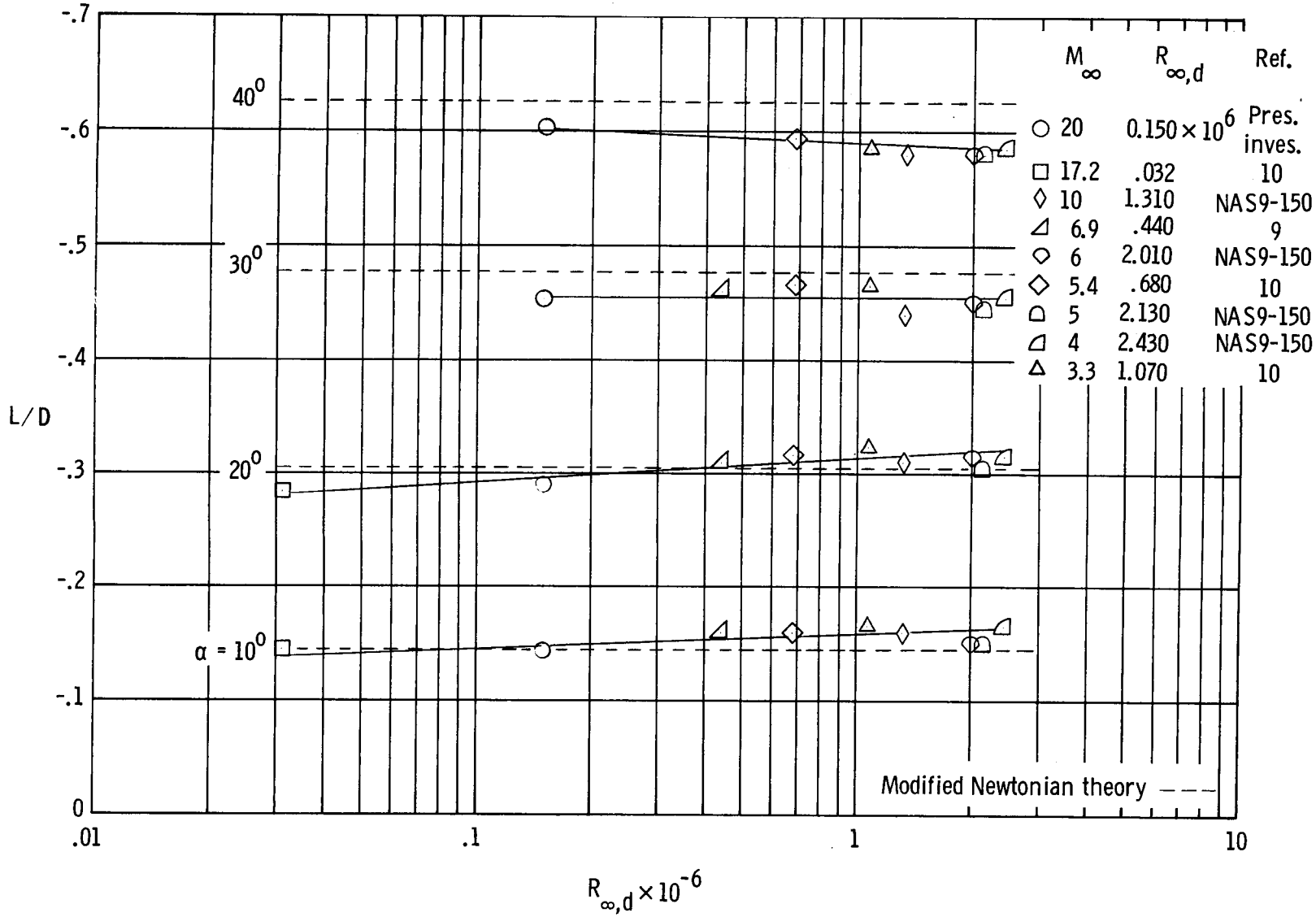

(c) Variation of L/D with $R_{\infty,d}$.

Figure 7.- Concluded.

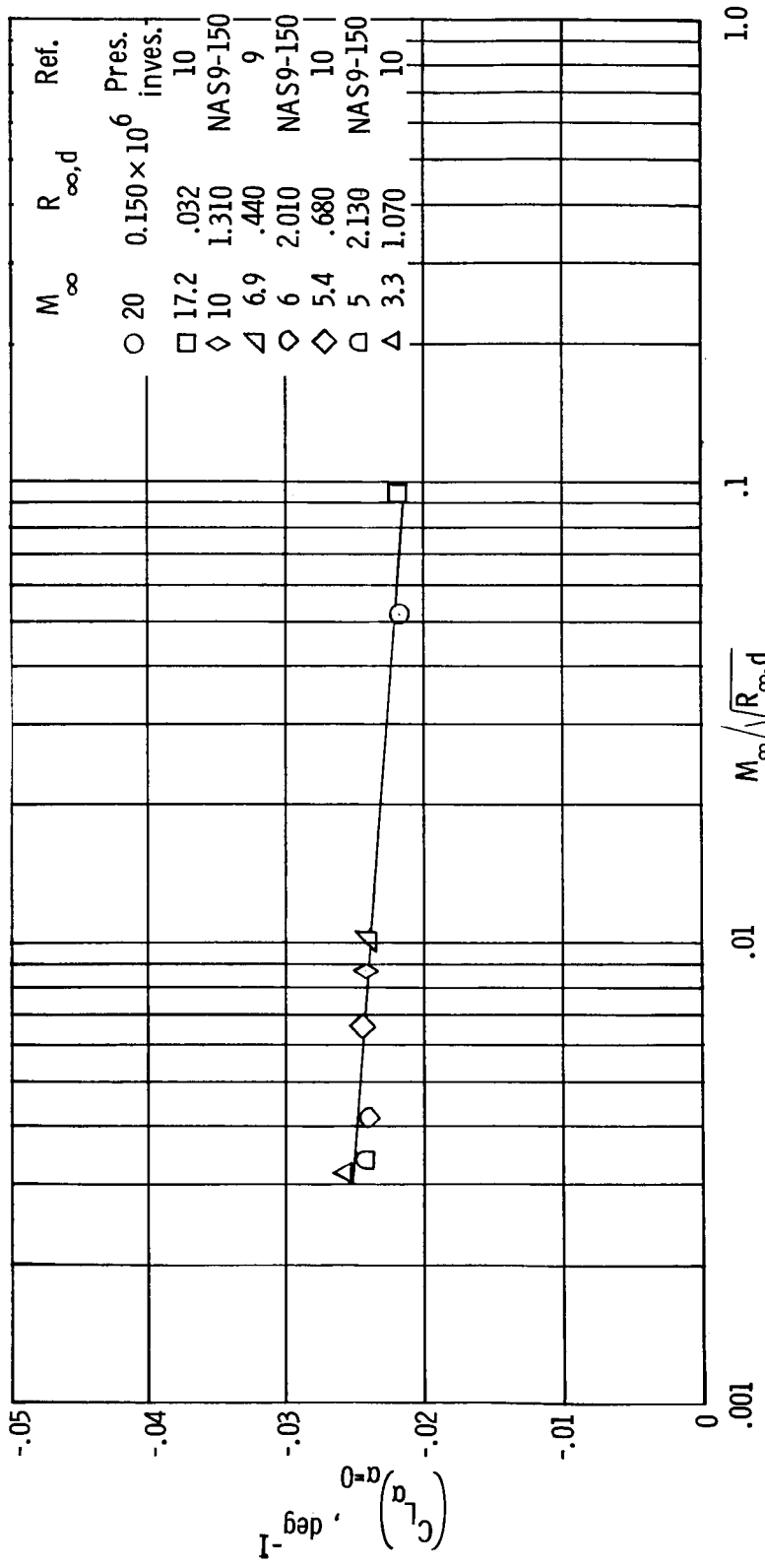

(a) Variation of $(C_{L_\alpha})_{\alpha=0}$ with $M_\infty/\sqrt{R_{\infty,d}}$.

Figure 8.- Study of lift-curve slope at zero angle of attack.

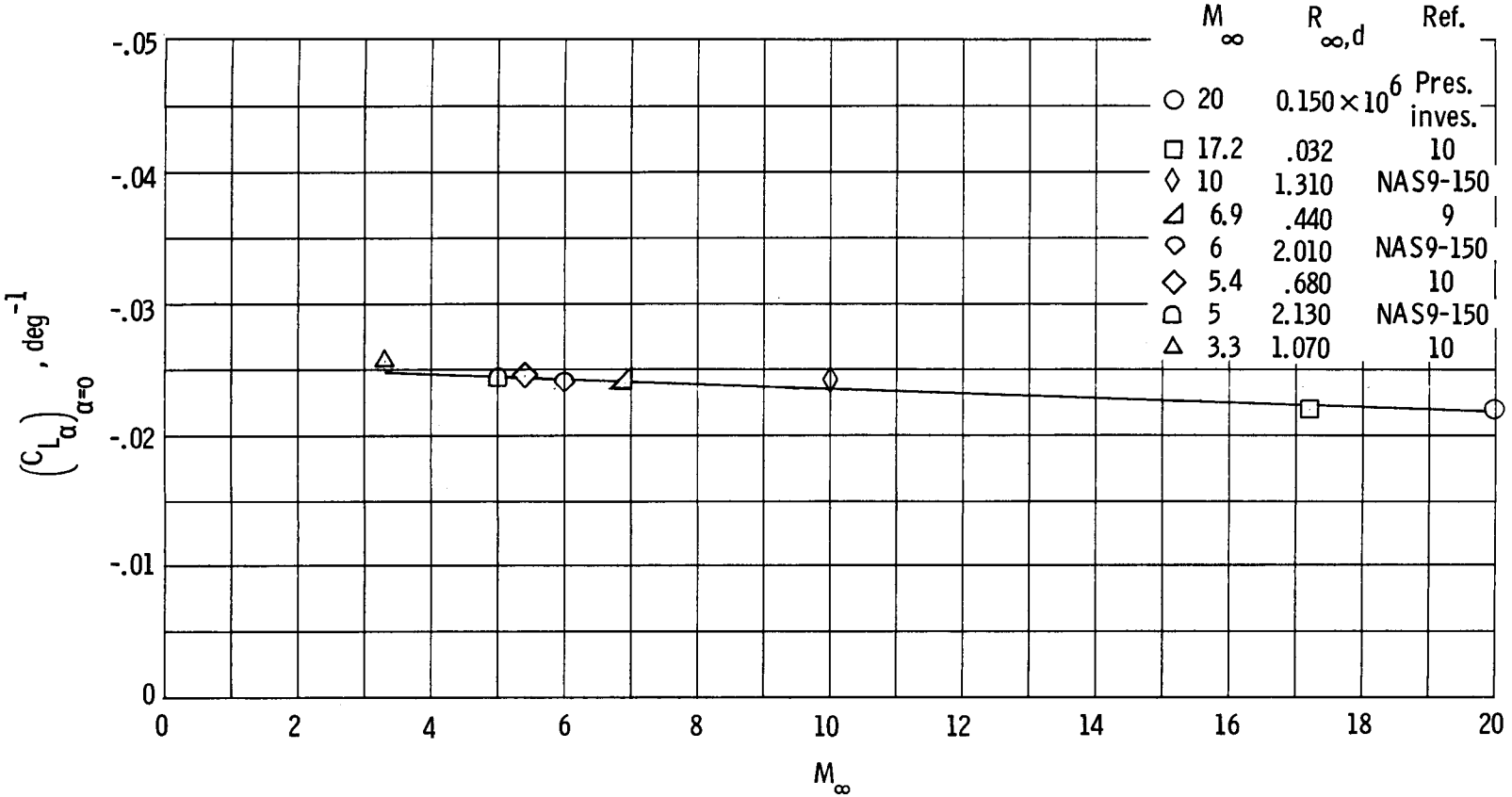

(b) Variation of $(C_{L_\alpha})_{\alpha=0}$ with M_∞.

Figure 8.- Continued.

(c) Variation of $\left(C_{L_\alpha}\right)_{\alpha=0}$ with $R_{\infty,d}$.

Figure 8.- Concluded.